The First International Scientific Conference of Health and Medical Specialties…… 15-16 April 2019

Kut Technical Institute / middle Technical University

Challenging key dogmas regarding skeletal muscle stem cells and their relationship to metabolism and regenerative capacity

Saleh Omairi[1, 3], Antonios Matsakas[2] and Ketan Patel[3]

1 Department of Anatomy and Biology, Medicine College, Wasit University, Kut, Iraq.
2 Hull York Medical School, Hull, United Kingdom.
3 School of Biological Sciences, University of Reading, Reading, United Kingdom.

Abstract

Skeletal muscle is a highly compliant tissue that is composed of muscle fibres, nerves, sensory cells, blood vessels and connective tissue. A central concept of skeletal muscle biology is the existence of an inverse relationship between muscle fibre size and its oxidative capacity which has been used to explain why small fibres are oxidative and large fibres glycolytic. Moreover, it has been shown that the numbers of satellite cells (the resident stem cells of skeletal muscle) are positively correlated with the oxidative muscle phenotype. Consistently, several studies have demonstrated that the genetic manipulations which induce muscle oxidative properties accelerate muscle regeneration capacity.

Observations of this work, firstly, challenge the notion of a constraint between skeletal muscle fiber size and oxidative capacity. Secondly, indicate the important role of the microcirculation in the regenerative capacity of a muscle even with low population of satellite cells.

I. INTRODUCTION

In mammalian skeletal muscle fibres are broadly characterised as slow or fast fibres, where slow fibres express the myosin heavy chain (MHC) isoform I, whereas fast fibres express MHC IIA, IIX and/or IIB. Slow fibres generally have a smaller cross-sectional area (CSA), contain more mitochondria which sustain a high oxidative capacity, and a denser microvascular network than fast fibres that rely predominantly on glycolysis for ATP production. Muscle fibres can change their phenotype, such as the expression of MHC, mitochondrial content and capillary supply in response to external stimuli (Pette and Staron, 2001). Skeletal muscles possess a high regenerative potential underpinned by the resident quiescent muscle progenitors cells known as satellite cells (SCs) (MAURO, 1961, Scharner and Zammit, 2011). The satellite cells reside between the basal lamina and sarcolemma of muscle fibre as a dormant myoblast, but they are activated in response to physiological stimuli for instance exercise, and pathological conditions such as injury and degenerative diseases (Gayraud-Morel et al., 2009). Subsequently, SCs enter the cell cycle and generate a committed population of muscle precursors that proliferate, differentiate and then either fuse with existing myofibres, repairing damaged muscle fibres, or fuse with each other to form new myofibres (Charge and Rudnicki, 2004, Gayraud-Morel et al., 2009). In parallel, a subset of SCs does not differentiate, but instead re-enter quiescence, thereby replenishing the stem cell pool (Zammit et al., 2004, Collins et al., 2005).

Muscle regeneration recapitulates many aspects of prenatal development, and it is an important homeostatic process of adult skeletal muscle. A number of chemicals have been utilised in order to investigate skeletal muscle degeneration/regeneration (Tajbakhsh and Cossu, 1997, Charge and Rudnicki, 2004). One of the most frequently used and reproducible method to induce muscle regeneration is based on cardiotoxin (CTX) injection (d'Albis et al., 1988). CTX is a snake venom fraction that induces muscle injury in a way similar to those observed in disease cases such as inflammatory myopathies (IMs) and muscular dystrophies (MDs) (Ramadasan-Nair et al., 2014). Furthermore, previous work has shown that CTX induces degeneration in the muscle fibres, but do not affect blood vessels, muscle innervation, extracellular matrix (ECM) content and muscle resident stem cells (SCs) (Shi and Garry, 2006). Alternatively, skeletal muscle degeneration/regeneration can be investigate by using other techniques, such as muscle crushing (Jager et al., 2014, Chatterjee et al., 2015), or the administration of different chemicals, such as barium chloride (Cornelison et al., 2004).

A number of studies have demonstrated that the genetic manipulations which induce muscle oxidative properties accelerate muscle regeneration capacity (Li et al., 2007). We hypothesised that the increased oxidative capacity and microvascular network following superimposition of Estrogen related receptor gamma (*Errγ*) in the Myostatin null ($Mtn^{-/-}$) background muscles might enhance the regeneration capacity of these muscles. To test this hypothesis, we induced injury of the Tibialis Anterior (TA) muscles from male (Wild Type (WT), Myostatin null ($Mtn^{-/-}$) and Myostatin null / Estrogen related receptor gamma overexpression) ($Mtn^{-/-}/Err\gamma^{Tg/+}$)) mice at 12 weeks old age using cardiotoxin (CTX) (Naja mossambica mossambica) and assessed the progression of regeneration at two crucial time points; day three (D3) as the process of debris clearance is on-going and regeneration of fibres begins, day six (D6) when a robust fibre regeneration can be quantified.
Observations of this study show a greater degree of regeneration (number and size of newly formed (Embryonic Myosin Heavy chain) $eMHC^{+}$ fibres) in $Mtn^{-/-}/Err\gamma^{Tg/+}$ compared to either $Mtn^{-/-}$ or WT mice after six days of CXT injection. Furthermore, we show a lower amount of cell death in the regenerating areas of $Mtn^{-/-}/Err\gamma^{Tg/+}$ muscles than the other two cohorts.

II. Materials and Methods

Ethical approval

Experiments were performed under a project license from the United Kingdom Home Office in agreement with the Animals (Scientific Procedures) Act 1986. The University of Reading Animal Care and Ethical Review Committee (AWERB) approved all procedures. Animals were humanely sacrificed via Schedule 1 killing between 8:00–13:00.

Animal maintenance

Healthy C57Bl/6 WT, $Mstn^{-/-}$, $Mstn^{-/-}/Err\gamma^{Tg/+}$ mice were bred and maintained in accordance to the Animals (Scientific Procedures) Act 1986 (UK) and approved by the University of Reading in the Biological Resource Unit of Reading University. Mice were housed under standard environmental conditions (20–22°C, 12–12 hr light–dark cycle) and provided food and water ad libitum. We used male mice that were 4–5 months old for this study. Specific experimental group consisted of 5-8 mice.

Intramuscular (IM) injection of Cardiotoxin into TA muscle

Prior to anesthetising, the solution to be injected was prepared in 30G, 8 mm long 1 mL insulin needles (Insumed 3079264). Animals were anesthetised and the fur at anterior side of the hind leg, around the TA muscle was shaved to allow more accurate orientation. The first injection was carried out with an insertion point parallel to the muscle, at the distal end of the anterior part of the TA. The needle was inserted approximately 7 mm into the muscle and 10 µL of solution was injected. The following two injections were carried out with insertion points vertical to the leg, lateral to the left and right of the proximal end of the TA, with 10 µL solution injected in both sites. In total, 30 µL of 50 µM Cardiotoxin from *Naja mossambica mossambica* was injected into the right TA, and 30 µL of sterile 1 x PBS was injected into the left TA muscles of all mice. Following injection, the animals were returned to their cages and allowed to recover from the anesthesia. The mice were closely monitored for at least 30 minutes to ensure full recovery. The animals were allowed to convalesce before being culled at tow time pointes (day 3, and day 6), then TA muscles were dissected and snap frozen for analysis.

Immunohistochemistry

Muscles were dissected following cervical dislocation. Muscles were snap frozen on a bed of isopentane cooled by liquid nitrogen. Frozen muscles Extensor Digitorum Longus (EDL), Soleus and Tibialis anterior (TA)) were mounted for cryo-sectioning in Tissue Tech freezing medium (Jung) cooled by dry ice/ethanol. 10 µm cryosections were taken using a Bright Cryostat (Bright PLC UK) and placed onto glass microscope slides. Tissue sections were air dried for 30 minutes at room temperature (RT) and either used immediately or stored at -80^{o}C. Sections were washed three times in PBS prior to immunohistochemistry staining. Muscle sections were incubated in permeabilisation buffer solution (0.952 g Hepes, 0.260 g MgCl2, 0.584 g NaCl, 0.1 g Sodium azide, 20.54 g Sucrose and 1 ml Triton X-100 in 200 ml dH_2O) for 15 minutes at RT, before the application of block wash buffer (PBS with 5% foetal calf serum (v/v), 0.05% Triton X-100) for 30 minutes at RT.

Primary antibodies were pre-blocked in wash buffer for 30 minutes prior to application onto muscle sections overnight at 4°C. All secondary antibodies were pre-blocked in wash buffer for minimum of 30 minutes (in dark) prior to their application onto the slides. Sections were then incubated for 1 hr in the dark at room temperature. Finally, slides were mounted in fluorescent mounting medium, and myonuclei were visualised using (2.5µg/ml) 4, 6-diamidino-2-phenylindole (DAPI). Details of primary and secondary antibodies are given in Supplementary File.

Isolation of intact single myofibres of EDL muscle

The EDL muscle was placed in 1ml of 2% type 1 collagenase (2mg/ml) after dissection. 1ml collagenase was sufficient to digest both EDL muscles from one mouse. The bijous that contain the EDL muscles were incubated at 37°C, 5%CO_2. The tubes of EDL muscles were agitated gently every 15 minutes to augment the digest speed. After approximately 30 minutes, individual myofibres began to peel away from the muscle. By 1.5 - 2 hours, the bulk of the myofibres had separated from the muscle mass. Prior to transfer the myofibres into a sterile washing dish, the dish was coated with horse serum to prevent myofibres attach on plastic.

A stereomicroscope (Nikon SMZ1500) with under stage light source was used to visualise the myofibres. Bundles of myofibres were gently aspirated using the sterile glass pipette until single isolated myofibres were seen. To remove residual collagenase, the myofibres were washed twice in Dulbecco's Modified Eagle Medium (DMEM), and twice with Single Fibre Culture Medium (SFCM). Care was taken during the washing to ensure that not all media was removed which can lead to myofibres contracting and so rendering the tissue useless for analysis. At this point, myofibres were either fixed at time-zero (T0) or cultured for desire time point (maximum 72 hours). Fixed myofibres were stored in 1.5 ml clear microtubes (Axygen MCT-175-C-S) at 4°C. Details of primary and secondary antibodies are given in Supplementary File.

Single myofibre fixation and culture

Cells (single myofibres) were fixed using 4% PFA/PBS at a volume ratio of 1:1 (final concentration 2% PFA/PBS) in 1.5 ml clear microtubes. To remove the fixative solution after 15 minutes of incubation at room temperature, 1 x PBS was used for three washes each wash lasting 5 minutes before being stored at 4°C.

For culturing, single myofibres were transferred carefully using a sterile glass pipette into 12-well plate (approximately 20 fibres per well), then 1 ml of SFCM was subsequently added to each well. All wells were checked to contain intact myofibres and any myofibre bundles liberated. Plates were transferred to a humid incubator at 37°C, 5% CO_2 and incubated for the required time period. Once myofibres had been cultured for the desired time period they were fixed as above and stored in 1.5 ml clear microtubes at 4°C for immunocytochemistry.

Macrophage immunocytochemistry

For macrophages identification, the Vector Laboratories ImmPRESS^{TM} Excel Staining kit Peroxidase was used and the protocol with the kit being followed.

Muscle sections were transferred from -80 freezer to room temperature and left for 20 minutes for drying. Prior to fix with acetone, the sections were washed in 1 x PBS three times with each wash lasting 5 minutes. For quenching of endogenous peroxidase activity, the sections were incubated with BLOXALL blocking solution for 10 minutes. Another two three minutes washes in 1 x PBS were performed before the slides being incubated with 2.5% of Horse Serum for 20 minutes. Primary antibody F4.80 (rat anti-mouse, BioRad MCA497R) was diluted in washing buffer prior to incubate on the muscle sections overnight. The slides washed twice in 1 x PBS each wash lasting three minutes before being incubated with Amplifier antibody for 15 minutes, washed a further twice in 1 x PBS three minutes each, and incubated for 30 minutes with ImmPRES Excel reagent. The sections were again washed twice with 1 x PBS for 5 minutes each prior to incubate with ImmPACT DAP *EqV* for 2-10 minutes and keep monitoring the stain develop till get the desire intensity. Another two washes in 1 x PBS each wash lasting 5 minutes were performed before slides being rinsed in tab water for 2 minutes. The sections were dehydrated in series concentrations of ethanol (70%, 90%, 100% and 100%) 30 seconds each before two washes in xylene for 30 seconds each. The slides were then mounted using DPX mounting media and covered with cover slip.

Succinate dehydrogenase (SDH) staining

Transverse muscle sections were incubated for 3 minutes at room temperature in a sodium phosphate buffer containing 75mM sodium succinate (Sigma), 1.1mM Nitroblue Tetrazolium (Sigma) and 1.03mM Phenazine Methosulphate (Sigma). Samples were then fixed in 10% formal-calcium and cleared in xylene prior to mounting with DPX mounting medium (Fisher). Photographic quantification of the samples was performed on a Zeiss Axioskop2 microscope mounted with an Axiocam HRc camera. Axiovision Rel. 4.8 software was used to capture the images.

RT-PCR

Frozen muscles were pulverised and solubilised in TRIzol (Fisher) using a tissue homogeniser. RNA was isolated and purified using a chloroform followed by isopropanol precipitation, in the RNAeasy Mini Kit (Quigen, Manchester, UK). RNA concentrations were measured using the Nanodrop 2000 (Thermo Scientific). Total RNA (5µg) was reverse-transcribed to cDNA with SuperScript II Reverse Transcriptse (Invitrogen) and analysed by quantitative real-time RT-PCR on a StepOne Plus cycler, using the Applied Biosystems SYBR-Green PCR Master Mix. Primers were designed using the software Primer Express 3.0 (Applied Biosystems). Relative expression was calculated using the $\Delta\Delta C_t$ method with normalization to the housekeeping genes *cyclophilin-B* and *hypoxanthine-guanine phosphoribosyltransferase (HPRT).* Specific primer sequences are given in Supplementary File.

Imaging and analysis

Fluorescence microscope (Ziess AxioImegar A1) was used to examine immunofluorescent stained sections, and images were captured using an Axiocam digital camera with Ziess Axiovision computer software version 4.8. To examine entire muscle, the images at mid-belly were reconstructed using Adobe Photoshop CS3. ImageJ software was used for counting analysis. For the detection of differences in myofibres cross-sectional area (CSA), Ziess Axiovison software version 4.8 was used.

Statistical analysis

Data were presented as mean ± SE. Significant differences between two groups were performed by Student's t-test for independent variables. Differences among groups were analysed by one-way analysis of variance (ANOVA) followed by Bonferroni's multiple comparison tests as appropriate. Statistical analysis was performed on GraphPad Prisim software. Differences were considered statistically significant at $p < 0.05$ (one asterisk), $p < 0.01$ (two asterisks) or $p < 0.001$ (three asterisks).

III. RESULTS

Skeletal muscle mass following *Myostatin* deletion and *Errγ* overexpression on *Myostatin* null background mice

Once death had been ascertained, we examined the weight of hind limb muscles (EDL, Gastrocnemius, Soleus and TA) (n=10) of the three genotypic groups (WT, $Mstn^{-/-}$, $Mstn^{-/-}/Err\gamma^{Tg/+}$). In agreement with previous study by McPherron and Lee (McPherron and Lee, 1997), we found that all the examined hind limb muscles (n=10) of *Myostatin* null animals were heavier than the wild type. The EDL, gastrocnemius, soleus and TA muscles were in both $Mtn^{-/-}$ and $Mtn^{-/-}/Err\gamma^{Tg/+}$ approximately 43%, 44%, 47% and 70% larger than their WT counterpart respectively (Figure 1 and Table 1).

Importantly, the increase in muscle weight in *Myostatin* knockout mice was maintained following *Errγ* overexpression. Of particular note there was no significant difference in mass for any of the muscles from $Mtn^{-/-}$ and $Mtn^{-/-}/Err\gamma^{Tg/+}$ mice. These data show that in the absence of *Myostatin*, the skeletal muscles become bigger, and *Errγ* transgenic mice preserved the increase of muscle mass exhibited by *Myostatin* null mice (Figure 2).

Figure 1. Hind limb muscle mass of WT, *Mtn* and *Mtn:Eγ* mice

Displaying clear disparate of hind limb muscles size of (WT), *Myostatin* null (*Mtn*) and *Errγ* transgenic mice on the *Myostatin* null background (*Mtn:Eγ*) mice.

Male twelve-week old mice.

Table 1. Weight of hind limb muscles from WT, *Mtn* and *Mtn:Eγ* mice.

Muscle / Weight (mg)	WT	*Mtn*	*Mtn:Eγ*
Extensor Digitorum Longus	14.9±1	21.4±0.8	21.2±0.9

Gastrocnemius	195.3±5.5	284.5±15.8	276±10
Soleus	12.6±1	18.5±1	17.2±0.5
Tibialis Anterior	54±0.5	92.8±5.6	90.4±3.2

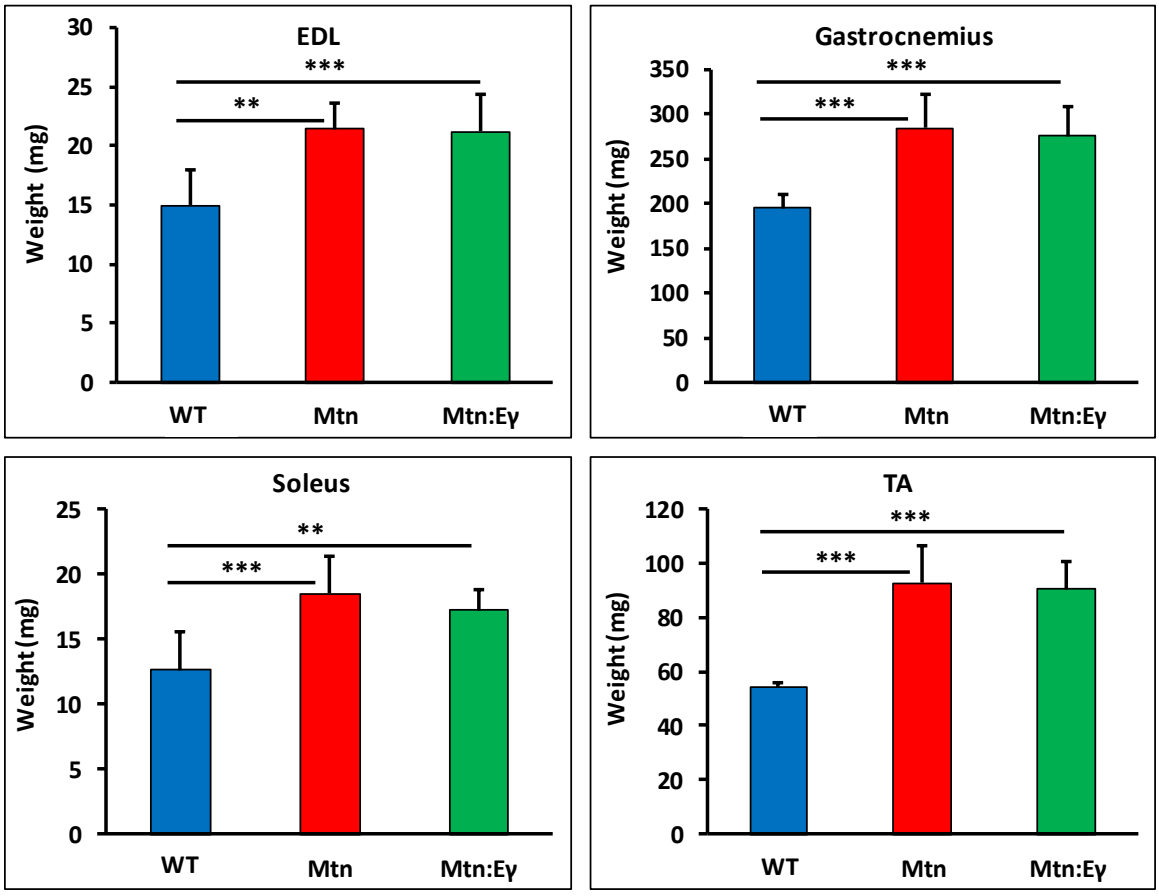

Figure 2. Muscle-specific expression of *Errγ* maintains hypertrophy features of *Myostatin* null background muscles

Quantification of skeletal muscle (EDL, gastrocnemius, soleus and TA) mass of wild type (WT), *Myostatin* null (*Mtn*) and *Errγ* transgenic mice on the *Myostatin* null background (*Mtn:Eγ*).

(*n* = 10) male twelve-week old mice per group; One-way ANOVA followed by Bonferroni's multiple comparison tests, ** = P<0.01 and ***= P<0.001.

Muscle fibre number and size

Skeletal muscle mass is usually influenced by both the number and size of the constituting fibres. We found that the introduction in *Errγ* into *Mstn*$^{-/-}$ did not significantly change the number of fibres normally seen in *Mstn*$^{-/-}$ muscles (Table 2 and Figure 3). The fibre sizes were also similar in the EDL of *Mstn-/-* and *Mstn*$^{-/-}$*Errγ*$^{Tg/+}$ lines.

Table 2. Myofibre number of Soleus and EDL muscles from WT, *Mtn* and *Mtn:Eγ* mice. All data are show as mean±SEM.

Muscle	Genotype	Average total fibre number
Extensor digitorum longus (EDL)	WT	882±32
	Mtn	1127±29
	Mtn:Eγ	1010±36
Soleus	WT	721±46
	Mtn	890±28
	Mtn:Eγ	896±47

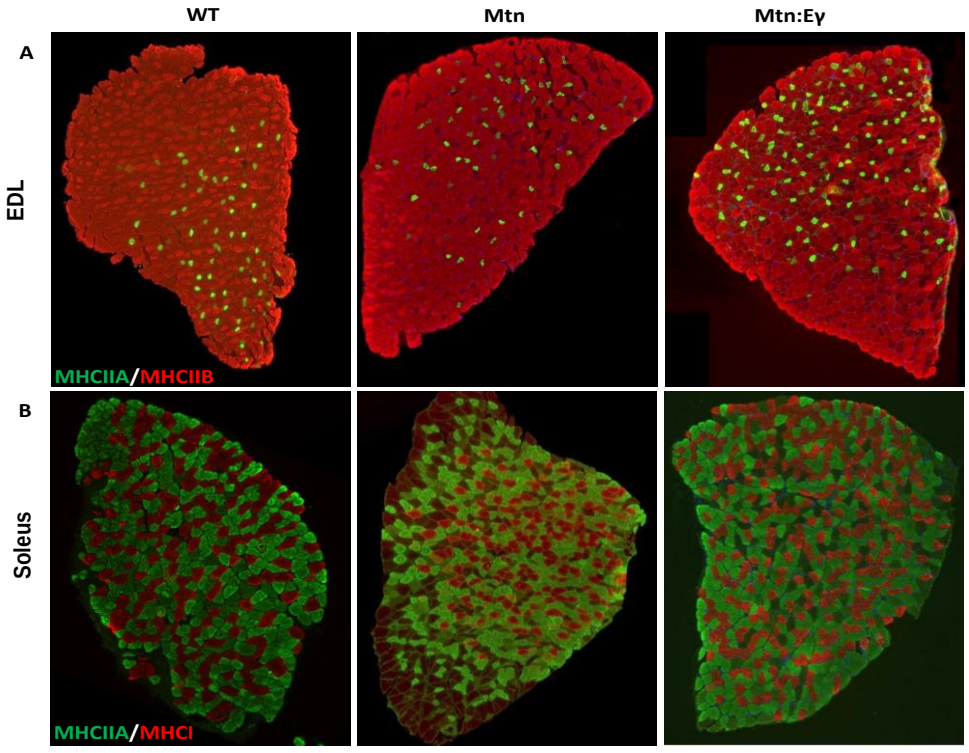

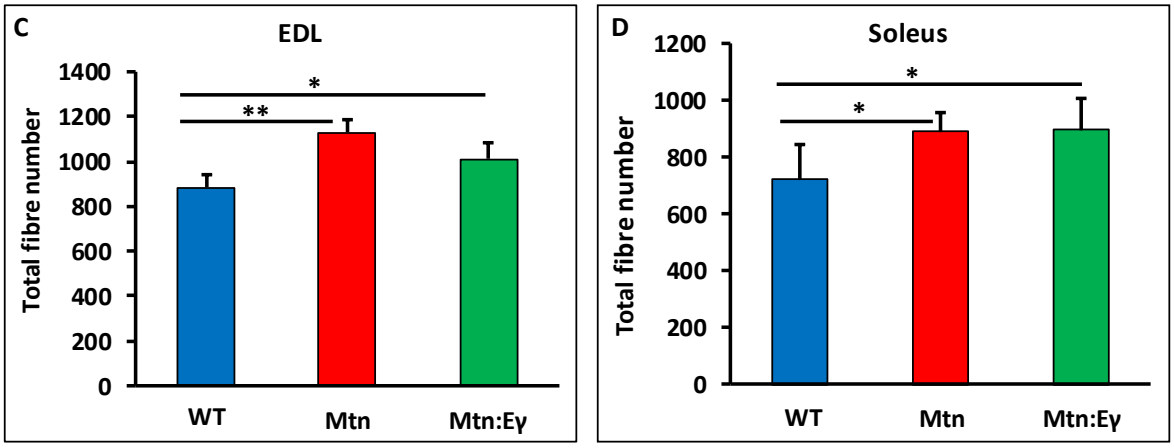

Figure 3. *Myostatin* deletion increased muscle fibres number and *Errγ* overexpression maintained this increase.
Muscle-specific expression of *Errγ* didn't affect the hyperplasia of *Myostatin* null background muscles

(**A**) Immunohistochemical images of EDL muscles from WT, *Mtn* and *Mtn:Eγ* mice. Green fibres signify the expression of MHCIIA with MHCIIB appearing as red.

(**B**) Immunohistochemical images of soleus muscles from WT, *Mtn* and *Mtn:Eγ* mice. Green fibres signify the expression of MHCIIA with MHCI appearing as red.

(C) Quantification of total fibres number in EDL muscles.

(D) Quantification of total fibres number in soleus muscles.

(*n* = 5-8) male twelve-week old mice per group; One-way ANOVA followed by Bonferroni's multiple comparison tests, *=P<0.05, and **=P<0.01.

Next we examined muscle fibre cross-sectional area (CSA). We found that the fibre sizes were equivalent in muscles from *Mstn-/-* and $Mstn^{-/-}/Err\gamma^{Tg/+}$ mice. Of particular note, both fibres from $Mstn^{-/-}$ and $Mstn^{-/-}/Err\gamma^{Tg/+}$ mice were larger than their counterparts from WT mice (Figure 4).

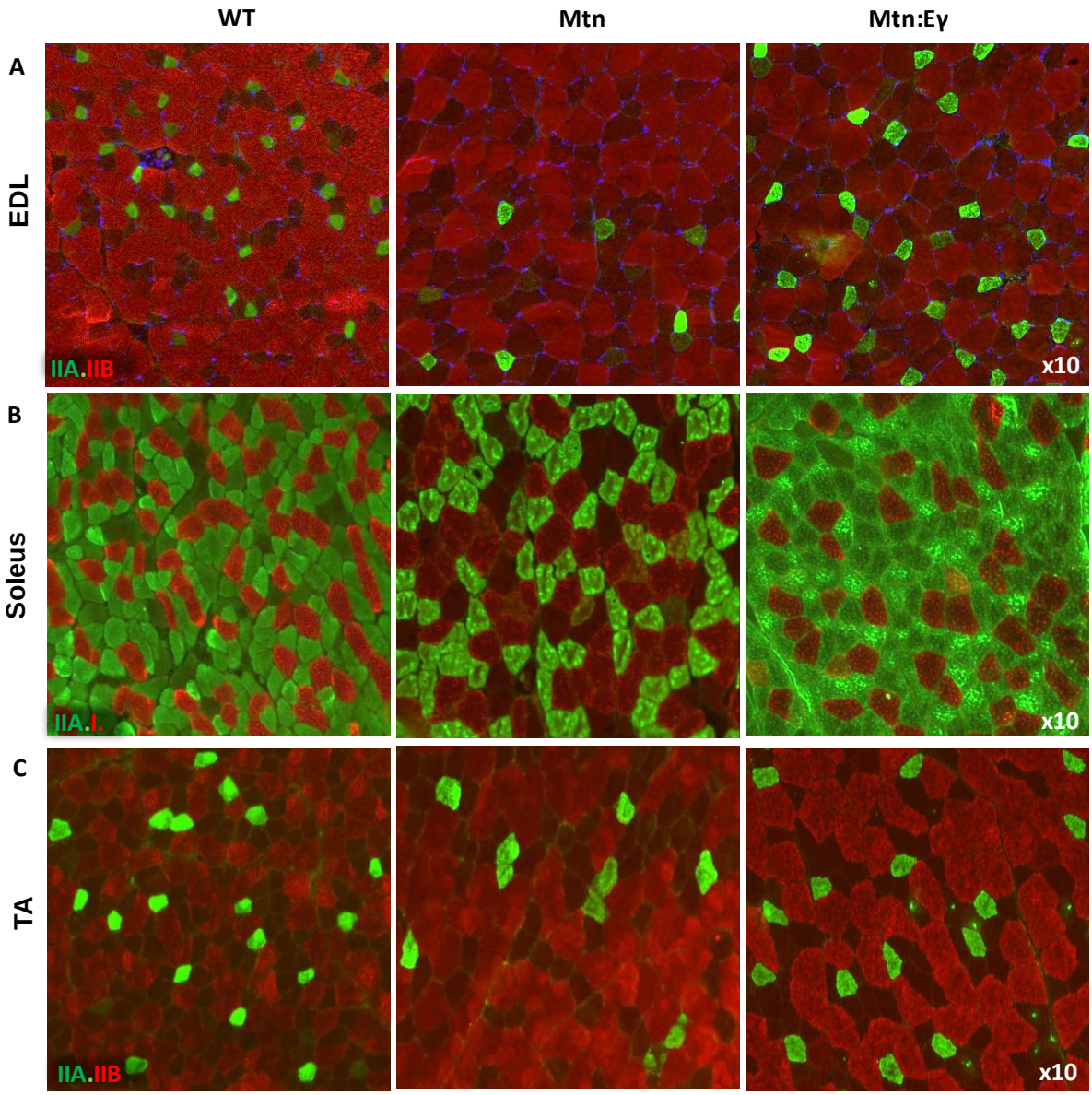

Figure 4. Myofibres size following *Myostatin* deletion and *Errγ* introducing into *Mtn*$^{-/-}$ mice

Muscle-specific expression of *Errγ* maintains muscle fibres hypertrophy exhibited by *Myostatin* null muscles. (**A**) Immunohistochemical images of EDL muscles from WT, *Mtn* and *Mtn:Eγ* mice. Green fibres signify the expression of MHCIIA with MHCIIB appearing as red. Non green and red fibres represent MHCIIX.

(**B**) Immunohistochemical images of soleus muscles from WT, *Mtn* and *Mtn:Eγ* mice. Green fibres signify the expression of MHCIIA with MHCI appearing as red.

(**C**) Immunohistochemical images of TA muscles from WT, *Mtn* and *Mtn:Eγ* mice. Green fibres signify the expression of MHCIIA with MHCIIB appearing as red. Non green and red fibres represent MHCIIX.

(n = 5-8) male twelve-week old mice per group.

$Err\gamma$ introducing into $Mtn^{-/-}$ mice induces robust increase of mitochondrion-associated enzyme succinate dehydrogenase (SDH) activity

We next examined the metabolic effects of expressing $Err\gamma$ in the $Mstn^{-/-}$ background. In all muscles examined, the number and intensity of SDH histochemical stain was lower in muscle from $Mstn^{-/-}$ compared to WT. However, upon over-expression of $Err\gamma$, the number and intensity of $Mstn^{-/-}$ muscle was restored to that of WT. Indeed, the number of SDH positive fibres was higher than even the WT in all three muscles albeit not reaching significance (Figure 5).

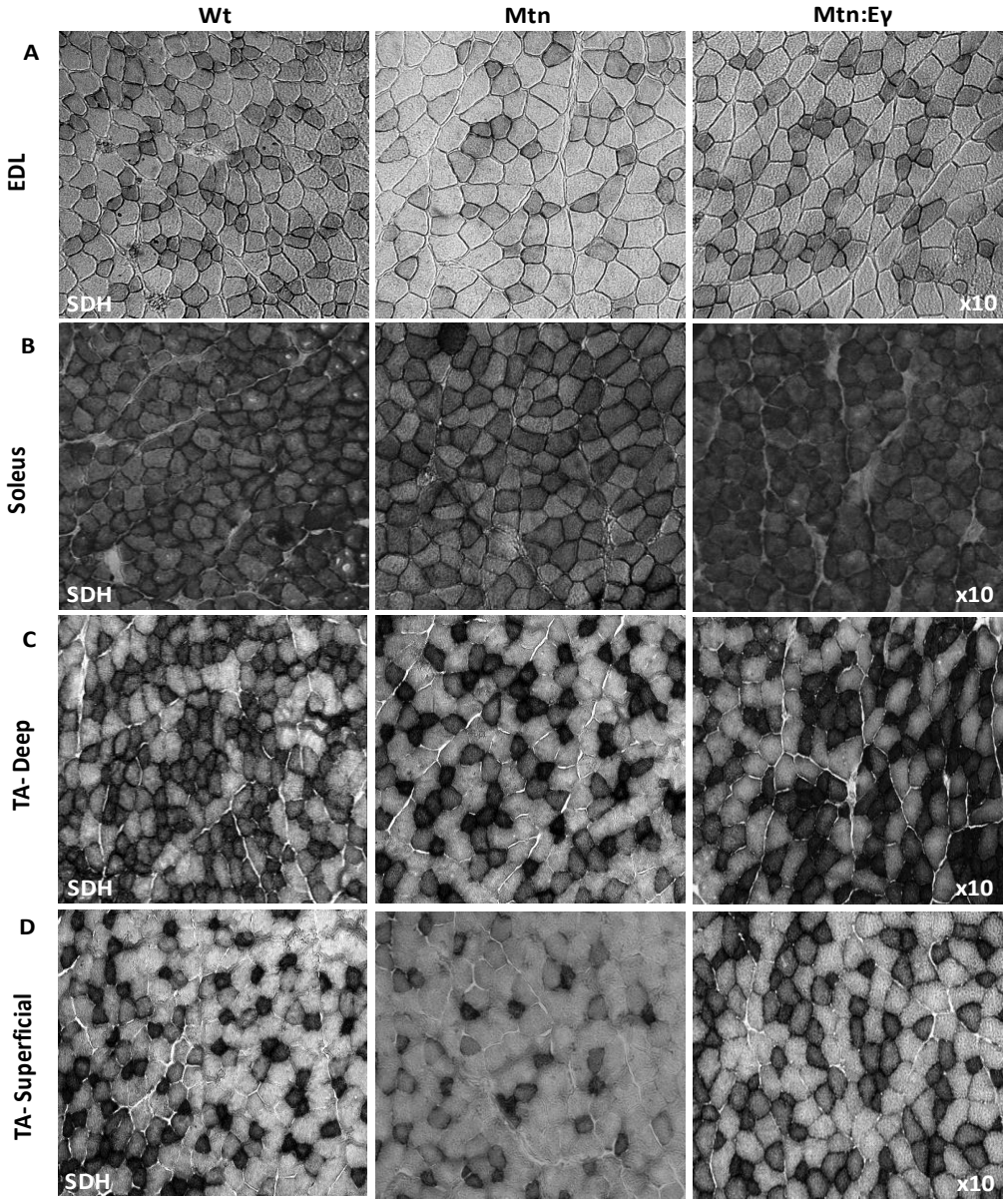

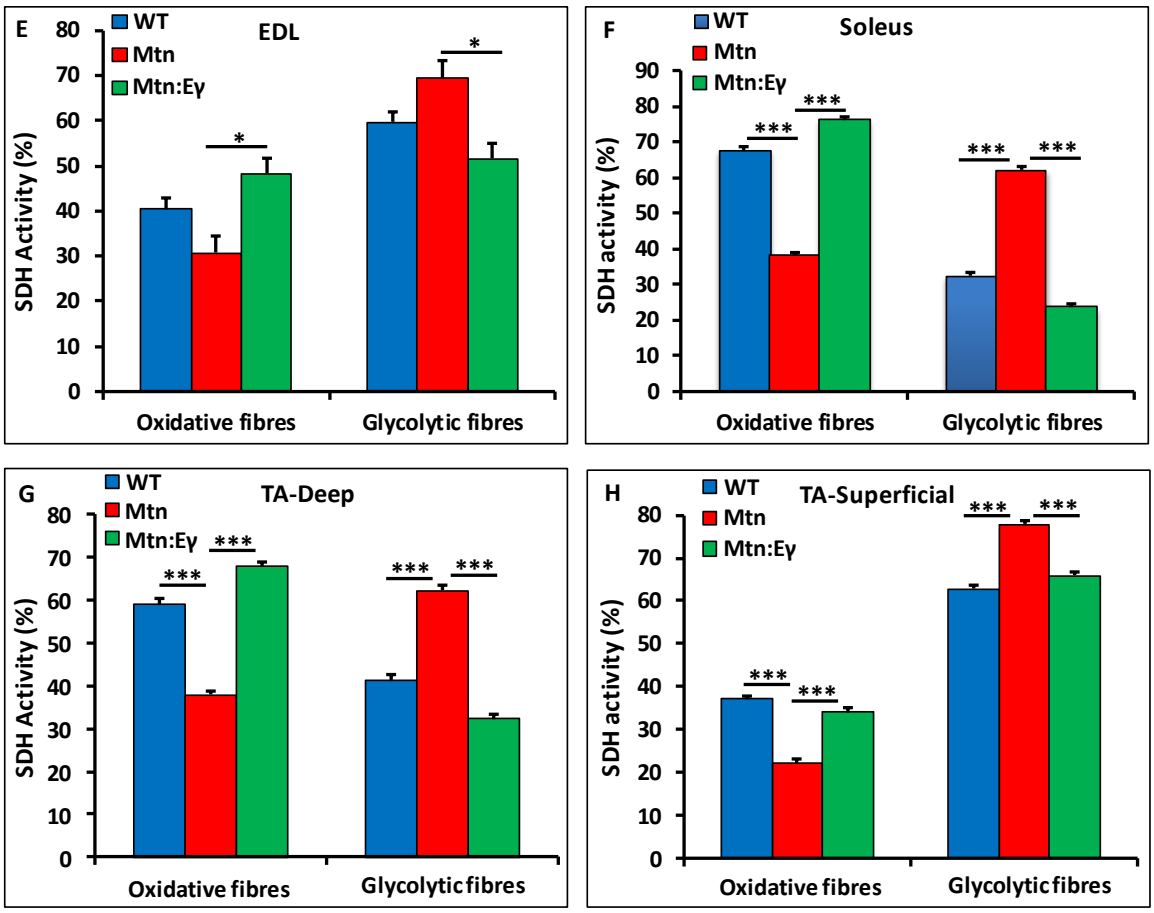

Figure 5. *Errγ* overexpression into *Mtn*$^{-/-}$ background muscle restores oxidative capacity to WT condition

Muscle-specific expression of *Errγ* normalizes the metabolic profile of *Myostatin* null mice (*Mtn*).

(**A – D**) Succinate dehydrogenase (SDH) staining Images of (EDL, soleus and TA-deep and superficial) muscles from WT, *Mtn* and *Mtn:Eγ* mice. Black fibres signify the SDH positive fibres (Oxidative fibres), and pale (white) fibres signify the SDH negative fibres (Glycolytic fibres).

(**E – H**) Quantification of SDH activity in EDL, soleus, TA-Deep and TA-Superficial muscles respectively.

(*n* = 5-8) male twelve-week old mice per group; One-way ANOVA followed by Bonferroni's multiple comparison tests, *=P<0.05 and ***= P<0.001.

Muscle-specific expression of *Errγ* is efficacious to promote angiogenesis program in a muscle lacking *Myostatin*.

A number of studies have established that the capillary density per muscle fibres is related to myofibre size, therefore an increase in the capillary number that follows a similar time course as the hypertrophy, is required (Degens et al., 1992, Plyley et al., 1998). Several other studies have recognised *Errγ* as a key transcriptional regulator that regulates the intrinsic vascular features and oxidative metabolism in the skeletal muscle (Rangwala et al., 2010, Narkar et al., 2011). Here we sought to determine whether the restoration of muscle oxidative capacity followed *Errγ* introducing into $Mtn^{-/-}$ mice would be accompanied by increasing of factors related to the microvascular supply of the muscle that known to regulate angiogenesis program. We found that the expression of endothelial mitogenic factors (*Vegf-α165* (Vascular endothelial growth factor α 165), *Vegf-α189* (Vascular endothelial growth factor α 189) and *Fgf1* (Fibroblast growth factor 1) was lower in the muscles of $Mtn^{-/-}$ than WT mice, but similar in $Mtn^{-/-}/Err\gamma^{Tg/+}$ and WT mice (Figure 6).
We next examined whether muscle-specific *Errγ* overexpression into $Mtn^{-/-}$ mice in addition to its potential to hold the increase of muscle fibre size and promote the oxidative capacity, could induce blood vessels formation to match the increased size and oxidative demands of the muscles. To test this, we examined TA muscle sections (n=5-8) from WT, $Mtn^{-/-}$ *and* $Mtn^{-/-}/Err\gamma^{Tg/+}$ mice for (CD31) expression, an endothelial cell marker that is routinely used to identify blood vessels (Figure 7A).

We found that capillary to fibre ratio (C:F) was the lowest in TA muscle sections from $Mtn^{-/-}$ mice, and the highest in those of $Mtn^{-/-}/Err\gamma^{Tg/+}$ mice. More specifically, muscles lacking *Myostatin* showed a significant decrease in a number of blood capillary per muscle fibre (1.3 blood vessels per myofibre) compared to control muscles (1.8 blood vessels per myofibre). However, *Errγ* overexpression in a muscle-specific manner markedly increased the number of blood vessels per each muscle fibre (2.6 blood vessels per myofibre). Interestingly, muscles from $Mtn^{-/-}/Err\gamma^{Tg/+}$ mice showed higher (C:F) ratio not only than those from *Myostatin* null, but also exceeded those of WT mice (Figure 7B).

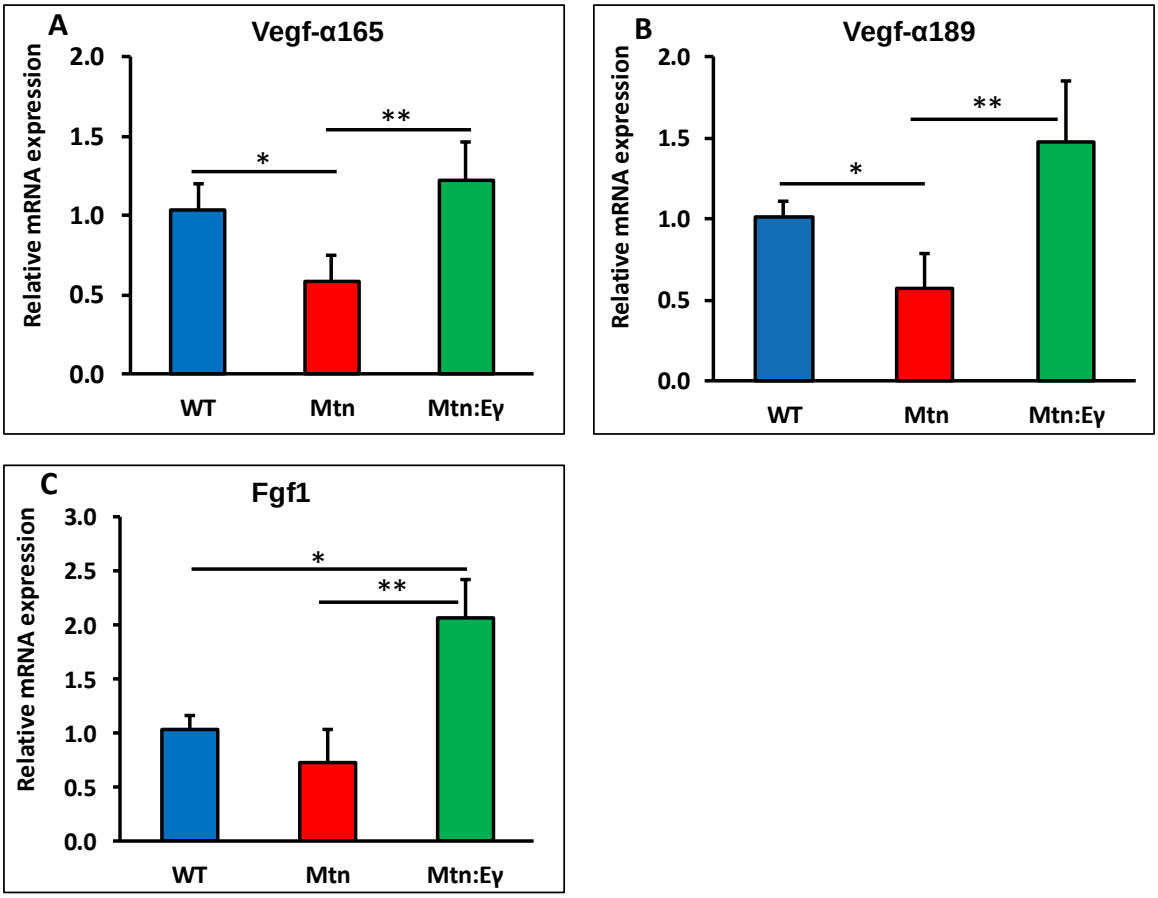

Figure 6. Molecular reprogramming of *Myostatin* null muscle by *Errγ* overexpression.

Errγ introducing into *Mtn* mice significantly increases expression levels of biomarker genes that regulate angiogenesis program

(A) Quantification of *Vegf-α 165* gene expression.

(B) Quantification of *Vegf-α 189* gene expression.

(C) Quantification of *Fgf1* gene expression.

(*n* = 5-8) male twelve-week old mice per group; One-way ANOVA followed by Bonferroni's multiple

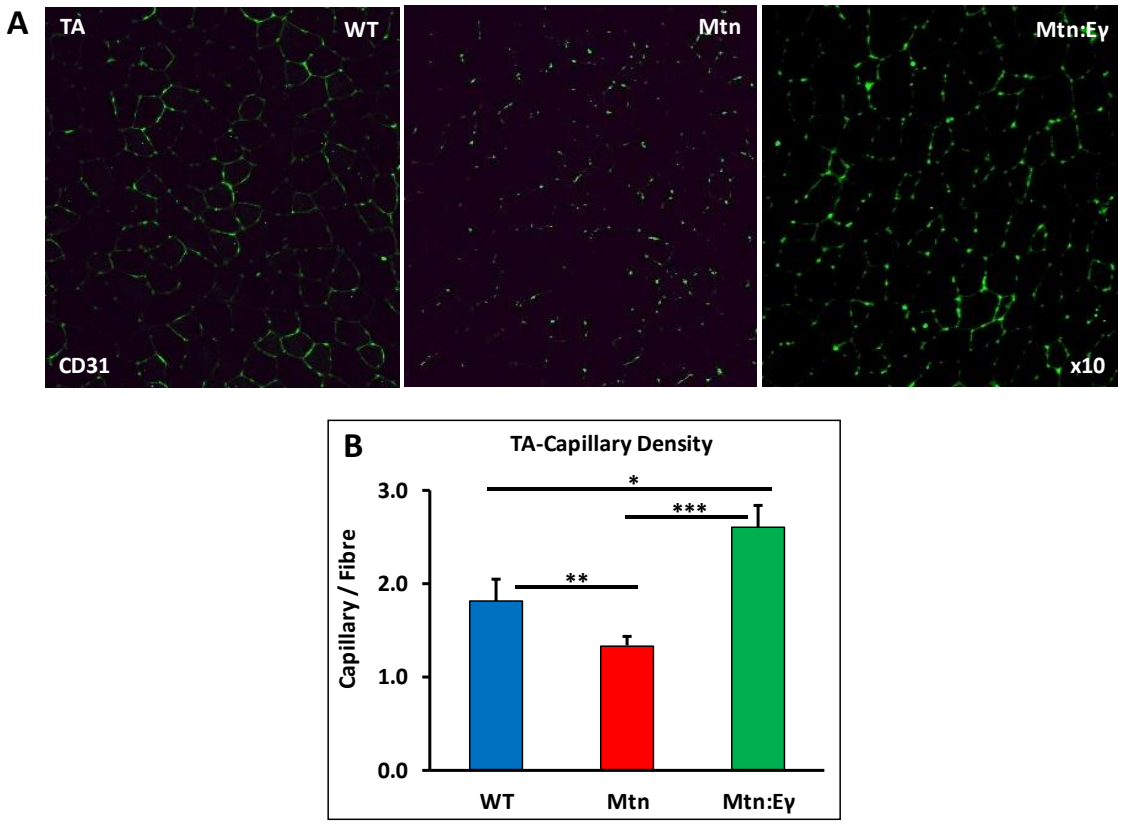

Figure 7. Revascularization of *Myostatin* null muscles following *Errγ* overexpression

Muscle-specific expression of *Errγ* normalizes capillary profile of *Myostatin* null mice (*Mtn*).

(**A**) Muscle capillary density determined by CD31 staining on TA muscle sections of WT, *Mtn* and *Mtn:Eγ* mice.

(**B**) Quantification of blood vessels per muscle myofibre in TA muscle sections.

(*n* = 5-8) male twelve-week old mice per group; One-way ANOVA followed by Bonferroni's multiple comparison tests, *=P<0.05, **=P<0.05 and ***= P<0.001.

Errγ overexpression into *Mtn*$^{-/-}$ mice does not rescue the reduction of satellite cells number in hyper-oxidative hypertrophic myofibres

We next examined consequences of Myostatin absence and *Errγ* introducing into *Mtn*$^{-/-}$ on individual muscle fibres. To do so, satellite cells on single muscle fibre from EDL muscles (n=5-8) from WT, *Mtn*$^{-/-}$ and *Mtn*$^{-/-}$/*Errγ*$^{Tg/+}$ mice were cultured and fixed in different time points, time zero (T0) and 48 hours culture (T48), thereafter immunostained with two myogenic markers (Pax7

and MyoD). Pax7 as a marker of satellite cells, and MyoD expressed as a marker of activated satellite cells and a key transcription factor for myogenic differentiation (Christov et al., 2007) (Figures 8A and 9A).

We found that deletion of *Myostatin* resulted in fewer satellite cells per myofibre (2.8 ± 0.3 and 10.9 ± 1) compared to WT (3.6 ±0.3 and 12.7 ± 0.9) at T0 and T48 time points respectively. At both time points, the number of satellite cells was even lower in the muscles of the $Mtn^{-/-}/Err\gamma^{Tg/+}$ mice (1.7 ± 0.1 and 4.1 ± 0.5) compared to the other genotypic groups (Figures 8A and B, and 9A and B). These results show that muscle-specific expression of *Errγ* in the $Mtn^{-/-}$ does not attenuate the deficit of satellite cell numbers that follows *Myostatin* ablation.

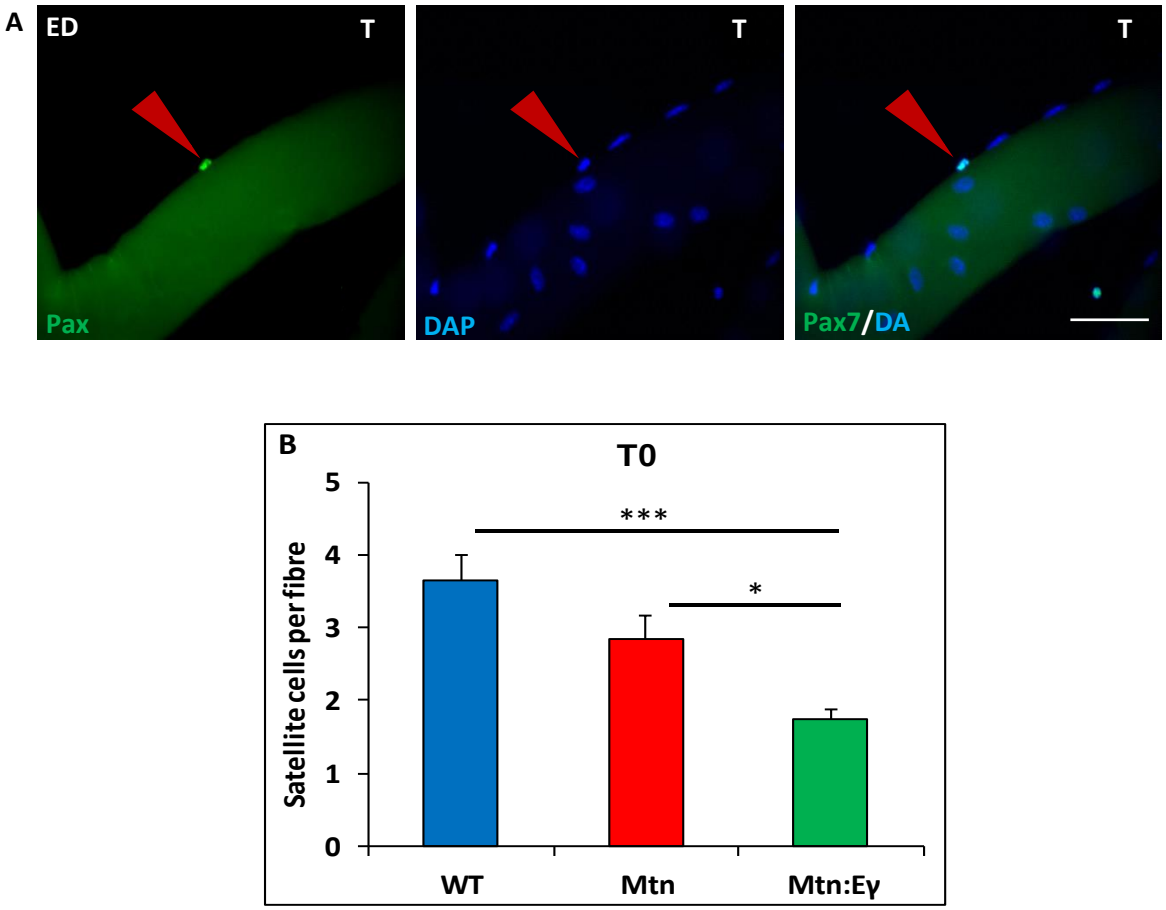

Figure 8. Fewer number of Satellite cells in EDL myofibre of *Mtn:Eγ* than other genotypic groups

Hypertrophied oxidative muscle developed through introduction of *Errγ* on the muscle of *Myostatin* null mice (*Mtn*) shows depletion of satellite cells.

(A) Quiescent satellite cells stained for DAPI and Pax7 on freshly isolated (T = 0 hr) muscle fibres from the EDL muscles (arrowhead), scale 50µm.

(B) Quantification of satellite cell number on freshly isolated EDL muscle fibres of WT, *Mtn* and *Mtn:Eγ* mice. Fibres were from 5-8 male twelve-week old mice per group; One-way ANOVA followed by Bonferroni's multiple comparison tests, *= P<0.05 and ***= P<0.001.

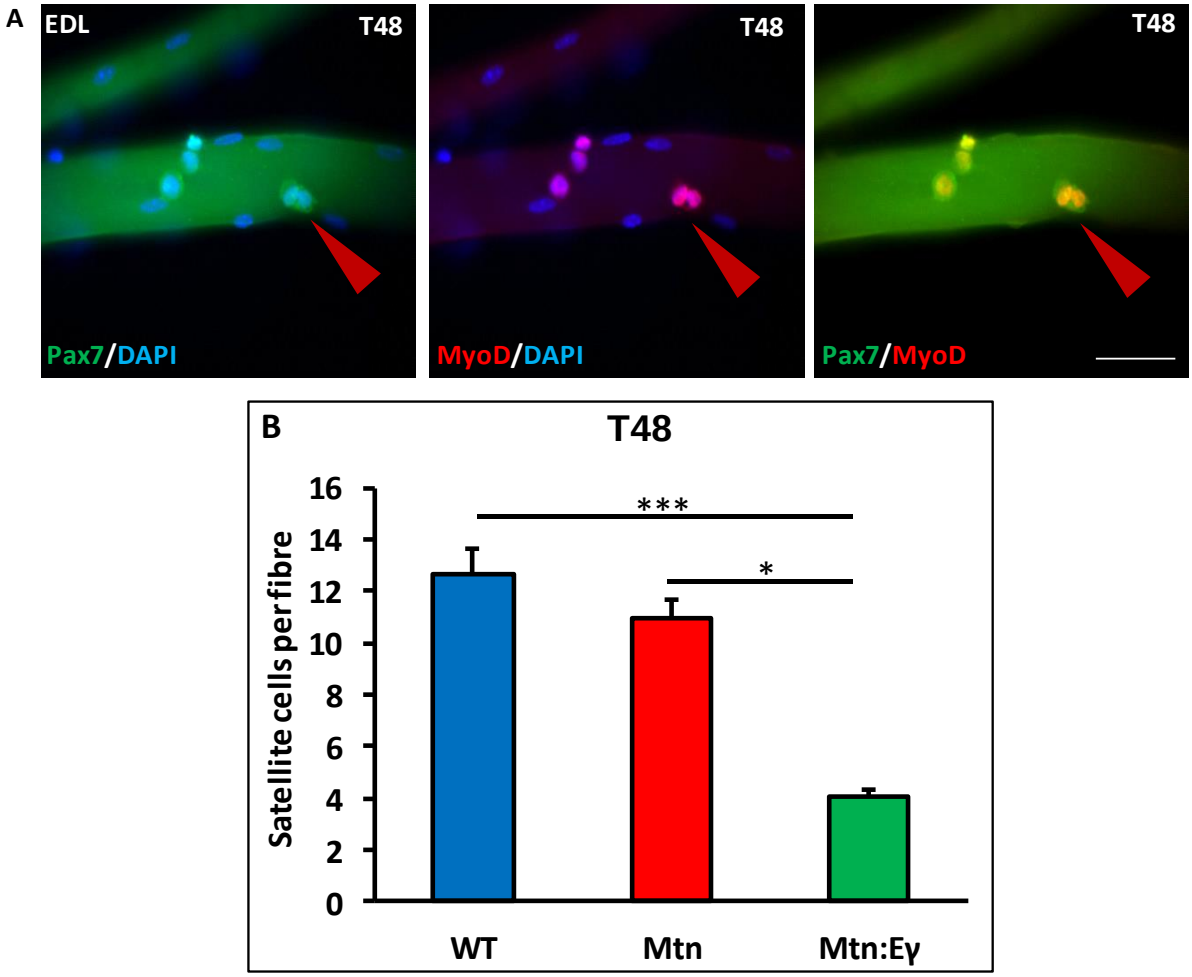

Figure 9. Muscle-specific expression of *Errγ* does not influence the satellite cell number

Hypertrophied oxidative muscle developed through introduction of *Errγ* on the muscle of *Myostatin* null mice shows depletion of satellite cells.

(A) Single muscle fibres from the EDL muscles after 48 hr in cell culture stained for DAPI, Pax7 and MyoD (arrowhead), scale 50µm.

(B) Quantification of satellite cell number on EDL muscle fibres at 48 hr.

Fibres were from 5-8 male twelve-week old mice per group; One-way ANOVA followed by Bonferroni's multiple comparison tests, *= P<0.05 and ***= P<0.001.

Skeletal muscle regeneration

Thus far all the changes in muscle resulting from over–expression of *Errγ* in the *Mstn*$^{-/-}$ were beneficial except for lower number of satellite cells (SC). In this section we determined the consequence of this deficit on the ability of skeletal muscle to regenerate, a process reliant on SC. To that end we induced injury of the TA using cardiotoxin and assessed the progression of regeneration at two crucial time points; day three (D3) as the process of debris clearance is ongoing and regeneration of fibres begins and day six (D6) when robust fibre regeneration can be quantified.

At D3 we found that the muscle clearance of dying fibres was slowest in *Mstn*$^{-/-}$ compared to the other two genotypes (Figure 10A-B). Clearance is mediated in part by macrophages, we found that the density of macrophages was highest in the muscle of *Mstn*$^{-/-}$/*Errγ*$^{Tg/+}$ compared to either *Mstn*$^{-/-}$ or WT (Figure 10C-D). Furthermore, we found that the TA from *Mstn*$^{-/-}$/*Errγ*$^{Tg/+}$ at the early stages of generation contained the highest number of committed muscle cells (Figure 10E-F).

By D6, we found evidence of newly regenerated muscle fibres by monitoring the expression eMHC in all cohorts. There were quantitative differences in the degree of regeneration with larger newly formed fibres found in *Mstn*$^{-/-}$/*Errγ*$^{Tg/+}$ compared to with *Mstn*$^{-/-}$ or WT (Figure. 11A-B) and a more advanced removal of dying fibres in *Mstn*$^{-/-}$/*Errγ*$^{Tg/+}$ than in Mstn$^{-/-}$ (Figure 11C-D). We also found evidence for a lower amount of cell death in the regenerating areas of *Mstn*$^{-/-}$/*Errγ*$^{Tg/+}$ than *Mstn*$^{-/-}$ or WT mice, by examining the density of cells expressing cleaved (activated) caspase 3 (Figure 11 E-F).

At D6 Macrophage activity was still highest in the muscle of *Mstn*$^{-/-}$/*Errγ*$^{Tg/+}$ compared to either *Mstn*$^{-/-}$ or wild type (Figure 11G-H) as were the number of committed (MyoD^{+}/Pax7) muscle progenitor cells (Figure 11I-J). These results show that even though the muscles of *Mstn*$^{-/-}$/*Errγ*$^{Tg/+}$ have fewer SCs than the muscles of the WT and *Mstn*$^{-/-}$ mice, their muscle regenerating capacity exceeds that of both *Mstn*$^{-/-}$ and WT mice.

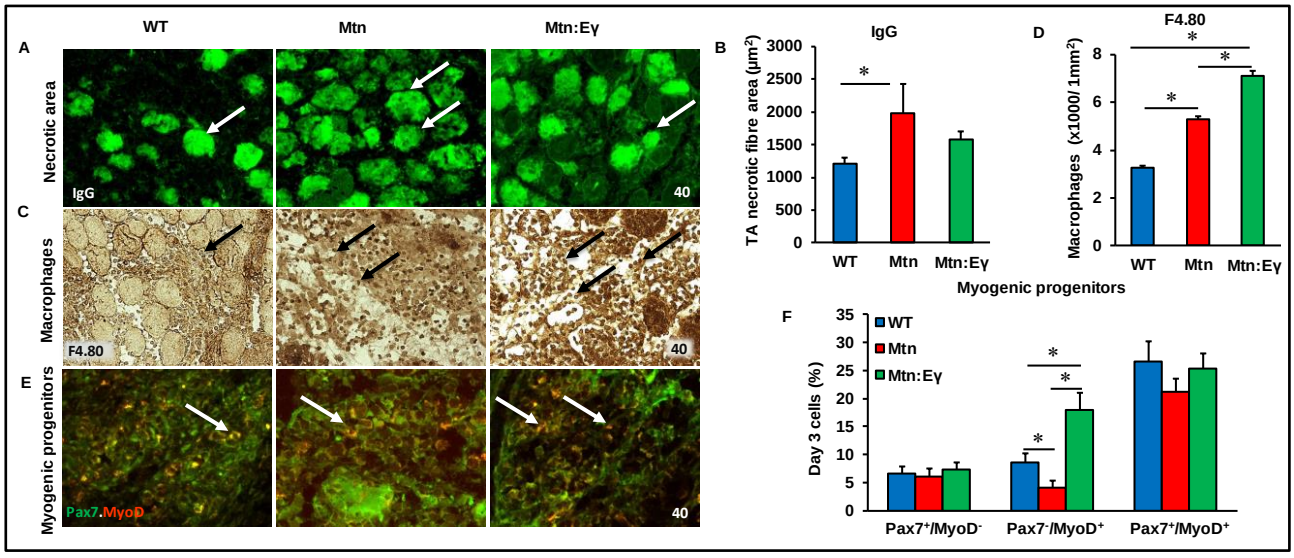

Figure 10. Skeletal muscle regeneration at day 3 is accelerated by the expression of *Errγ* in *Myostatin* null mice through enhanced macrophage and satellite cells activity.

(A) Muscle necrotic fibres (white arrows) visualized by IgG staining on damaged TA muscles of WT, *Mtn* and *Mtn:Eγ* mice at day 3 after CTX injection.

(**B**) Quantification of dying fibre number after 3 days of CTX injection.

(C) Macrophage infiltration in the TA muscle using an F4.80 antibody at day3 (arrows).

(D) Quantification of macrophage density in damaged muscles**.**

(E) Myogenic progenitors at day3. Pax7 detection in green, Myo D expressing cells in red (arrows).

(F) Quantification of uncommitted muscle cells ($Pax7^{+}/MyoD^{-}$)**,** precursors ($Pax7^{+}/MyoD^{+}$), and committed ($Pax7^{-}/MyoD^{+}$).

(*n* = 5-8) male twelve-week old mice per group; One-way ANOVA followed by Bonferroni's multiple comparison tests, *=$p<0.05$ and ***= $p<0.001$.

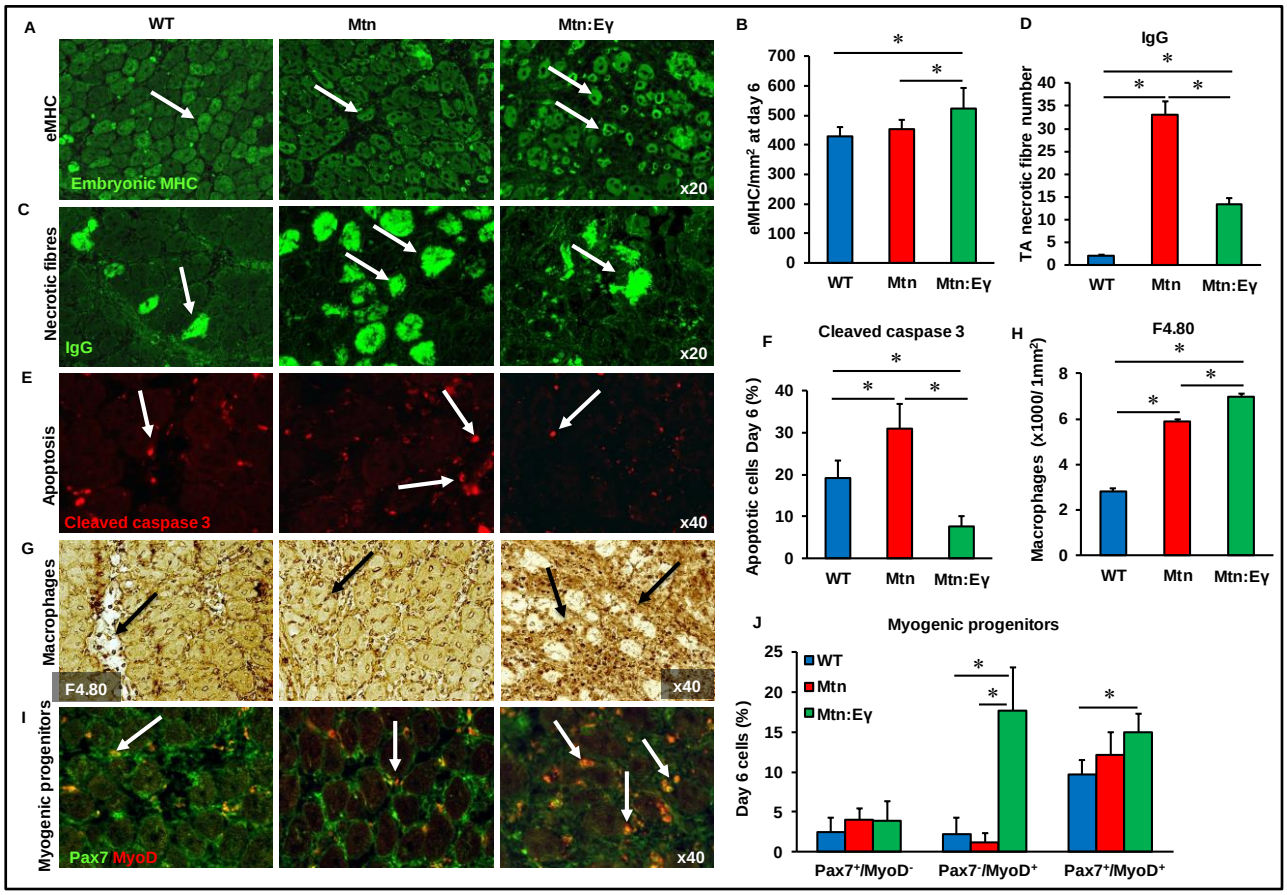

Figure 11. Skeletal muscle regeneration at day 6 is accelerated by the expression of *Errγ* in *Myostatin* null mice through enhanced macrophage and satellite cells activity.

(A) Expression of eMHC on day 6 (arrows).

(**B**) Quantification of regeneration muscle fibres on day 6.

(C) Necrotic fibres at days detected via infiltrated fibre IgG profiling (arrows).

(D) Quantification of dying muscle fibres at day 6.

(E) Cleaved caspase 3 staining at day 6 as a marker of apoptosis (arrows).

(F) Quantification of apoptosis density at day 6.

(G) Macrophage infiltration in the TA at day 6 (arrows).

(H) Quantification of Macrophage infiltration at day 6.

(I) Myogenic progenitors at day 6. Pax 7 detecting in green, MyoD expressing cells in red (arrows).

(J) Quantification of uncommitted muscle cells ($Pax7^{+}/MyoD^{-}$)**,** precursors ($Pax7^{+}/MyoD^{+}$), and committed ($Pax7^{-}/MyoD^{+}$) muscle cells at day6.

(*n* = 5-8) male twelve-week old mice per group; One-way ANOVA followed by Bonferroni's multiple comparison tests, *=p<0.05 and ***= p<0.001.

IV. Discussion

Classical training experiment has established that skeletal muscles have limited capacity to get a commensurate improvement of their mass (hypertrophy) and fatigue resistance (Hickson, 1980). In consistence, previous work has referred to the plasticity nature of skeletal muscle that capable to alter almost all its features at metabolic, ultrastructure and molecular levels in response to environmental stimuli or gene mutation (Pette and Staron, 2001). Myostatin is a member of the TGF-β family of secreted protein that been defined as a potent inhibitor of muscle development, and mutation of its gene leads to hypertrophic fast contracting fibres (McPherron and Lee, 1997, Amthor et al., 2007). The higher than normal fatigability of the muscle could be attributable to the lower level of oxidative capacity as consequent to deletion of *Myostatin* in the germline (Amthor et al., 2007). To alleviate this oxidative deficit in $Mstn^{-/-}$ mice we introduced the expression of *Errγ* into skeletal muscle. This gene is highly expressed in tissues with a high oxidative capacity, such as heart, kidney, brain and slow oxidative skeletal muscle where it has been demonstrated to trigger mitochondrial biogenesis (Heard et al., 2000, Narkar et al., 2011, Giguere, 2008). Such an introduction of *Errγ* overexpression that would increase oxidative capacity on a $Mstn^{-/-}$ background that is associated with hypertrophy challenges the trade-off that is thought to exist between oxidative capacity and fibre size (Van der Laarse WJ, 1998).

The main observations of the present study are firstly that substantial hypertrophy can occur without a concomitant reduction in fibre oxidative capacity. This observation challenges the dogma that there is a revers correlation between muscle fibre size and oxidative capacity. Secondly, our results challenge the notion that slow oxidative muscle has a higher number of satellite cells than those are fast glycolytic.

In agreement with aforementioned findings (Girgenrath et al., 2005, Amthor et al., 2007), our study demonstrates that the key feature of $Mtn^{-/-}$ muscles is the lower SDH activity, indicative of a low muscle oxidative capacity. This combination of a low oxidative capacity and a large fibre size fits nicely with the concept of the trade-off between fibre size and oxidative capacity (Van der Laarse WJ, 1998). On the contrary, even our observations demonstrated no difference in fibre CSA between muscles from $Mtn^{-/-}$ and $Mtn^{-/-}/Err\gamma^{Tg/+}$ mice, the latter had significantly high SDH activity.

One of the key findings of our study is the characterization of skeletal muscle composed of large and oxidative fibres. A number of studies have suggested that fibres that rely on oxidative phosphorylation limit their size in order that oxygen from the blood supply diffuses efficiently into the cells and to the mitochondria for ATP production (Kinsey et al., 2007, Van der Laarse WJ, 1998). The large fibers with a low oxidative capacity in $Mstn^{-/-}$ mice conform to this concept and even have a lower capillary supply per fibre. The latter is in contrast with models of hypertrophy where the increase in fibre size is accompanied with capillary proliferation that is, however, proportionally less than the increase in fibre size (Degens et al., 1992). The discrepancy between such observations and the lower number of capillaries in the $Mstn^{-/-}$ muscles maybe explicable by the lower oxidative capacity of the $Mstn^{-/-}$ muscles. During compensatory hypertrophy the time course of angiogenesis and fibre hypertrophy are similar (Egginton et al., 1998, Plyley et al., 1998), and the capillary supply to a fibre is related to the size of the fibre (Ahmed et al., 1997), such a

coupling between fibre size and capillary supply seems to be altered in the *Mstn*$^{-/-}$ mice. However, over-expression of *Errγ* in *Mstn*$^{-/-}$ increases the number of capillaries per fibre (See Fig. 7) (Narkar et al., 2011). An important finding here is that the angiogenesis programme promoted by muscle expression of *Errγ* is responsive to change in fibre size so that when a fibre grows, it stimulates the formation of blood vessels presumably to ensure optimal perfusion.

Interestingly, our study gives a new perspective on the relationship between metabolism, satellite cells number and their activity during regeneration. A number of studies have implied that slow muscles contain more satellite cells than fast ((Putman et al., 1999, Christov et al., 2007). In this study we show that in the EDL as the fibres transitioned from glycolytic to oxidative, the number of associated satellite cells was significantly reduced. We postulate that the absence of myostatin promotes myoblast fusion at the expense of SC. Furthermore, that over-expression of *Errγ* exacerbates this relationship. Severe depletion of satellite cells numbers has been reported to severely retard the process of muscle regeneration (Vasyutina et al., 2007, Schuster-Gossler et al., 2007).

Here we show that the depletion of satellite cells to less than 50% of their normal levels does not impact on skeletal muscle regeneration since they have a vast capacity to generate precursors which in most situation is never realized fully (Collins et al., 2005). Instead we suggest that oxidative environment established by *Errγ* is the key determinant in accelerating regeneration. Our work supports previous work showing that oxidative metabolism supports muscle regeneration (Lowrie et al., 1982). Findings of current study are in agreement with a number of studies showing that genetic manipulations leading to a greater oxidative capacity accelerate muscle regeneration (Li et al., 2007). One possible explanation for our results is our finding that *Errγ* promotes hyper-vascularization. Angiogenesis which is a key determinant in the muscle regeneration process. We suggest that the reduction of SC is off-set by the ability to promote vascularization and clearance of the necrotic tissues, allowing the small number of satellite cells to expand greatly to enact rapid repair. This hypothesis is supported by our data investigating both macrophage density and generation of myoblast in the *Mstn*$^{-/-}$/*Errγ*$^{Tg/+}$ mice.

In summary our work demonstrates that canonical views regarding muscle fibre size and metabolism can be genetically manipulated. The deviation from this relationship may be realized by the increased capillarization and oxidative capacity. Moreover, it is likely that the increased microvascular network plays a crucial role in muscle regeneration as the *Mstn*$^{-/-}$/*Errγ*$^{Tg/+}$ mice had even lower satellite cells number than *Mstn*$^{-/-}$ mice, yet a regenerative capacity even exceeded that of WT mice. In future we will determine whether it confers other advantages in particular the ability to confer resistance to obesity and sarcopenia.

SUPPLEMENTAL INFORMATION

Supplemental information includes details of antibodies (Primary and Secondary), and primers used in this study.

AUTHORS CONTRIBUTION

Conceptualization K.P. and S.O., Methodology S.O., Investigation S.O., Writing S.O., and Supervision K.P.

References

AHMED, S. K., EGGINTON, S., JAKEMAN, P. M., MANNION, A. F. & ROSS, H. F. 1997. Is human skeletal muscle capillary supply modelled according to fibre size or fibre type? *Exp Physiol,* 82**,** 231-4.

AMTHOR, H., MACHARIA, R., NAVARRETE, R., SCHUELKE, M., BROWN, S. C., OTTO, A., VOIT, T., MUNTONI, F., VRBOVA, G., PARTRIDGE, T., ZAMMIT, P., BUNGER, L. & PATEL, K. 2007. Lack of myostatin results in excessive muscle growth but impaired force generation. *Proc Natl Acad Sci U S A,* 104**,** 1835-40.

CHARGE, S. B. & RUDNICKI, M. A. 2004. Cellular and molecular regulation of muscle regeneration. *Physiol Rev,* 84**,** 209-38.

CHATTERJEE, S., YIN, H., NAM, D., LI, Y. & MA, K. 2015. Brain and muscle Arnt-like 1 promotes skeletal muscle regeneration through satellite cell expansion. *Exp Cell Res,* 331**,** 200-10.

CHRISTOV, C., CHRETIEN, F., ABOU-KHALIL, R., BASSEZ, G., VALLET, G., AUTHIER, F. J., BASSAGLIA, Y., SHININ, V., TAJBAKHSH, S., CHAZAUD, B. & GHERARDI, R. K. 2007. Muscle satellite cells and endothelial cells: close neighbors and privileged partners. *Mol Biol Cell,* 18**,** 1397-409.

COLLINS, C. A., OLSEN, I., ZAMMIT, P. S., HESLOP, L., PETRIE, A., PARTRIDGE, T. A. & MORGAN, J. E. 2005. Stem cell function, self-renewal, and behavioral heterogeneity of cells from the adult muscle satellite cell niche. *Cell,* 122**,** 289-301.

CORNELISON, D. D., WILCOX-ADELMAN, S. A., GOETINCK, P. F., RAUVALA, H., RAPRAEGER, A. C. & OLWIN, B. B. 2004. Essential and separable roles for Syndecan-3 and Syndecan-4 in skeletal muscle development and regeneration. *Genes Dev,* 18**,** 2231-6.

D'ALBIS, A., COUTEAUX, R., JANMOT, C., ROULET, A. & MIRA, J. C. 1988. Regeneration after cardiotoxin injury of innervated and denervated slow and fast muscles of mammals. Myosin isoform analysis. *Eur J Biochem,* 174**,** 103-10.

DEGENS, H., TUREK, Z., HOOFD, L. J., VAN'T HOF, M. A. & BINKHORST, R. A. 1992. The relationship between capillarisation and fibre types during compensatory hypertrophy of the plantaris muscle in the rat. *J Anat,* 180 (Pt 3)**,** 455-63.

EGGINTON, S., HUDLICKA, O., BROWN, M. D., WALTER, H., WEISS, J. B. & BATE, A. 1998. Capillary growth in relation to blood flow and performance in overloaded rat skeletal muscle. *J Appl Physiol (1985),* 85**,** 2025-32.

GAYRAUD-MOREL, B., CHRETIEN, F. & TAJBAKHSH, S. 2009. Skeletal muscle as a paradigm for regenerative biology and medicine. *Regen Med,* 4**,** 293-319.

GIGUERE, V. 2008. Transcriptional control of energy homeostasis by the estrogen-related receptors. *Endocr Rev,* 29**,** 677-96.

GIRGENRATH, S., SONG, K. & WHITTEMORE, L. A. 2005. Loss of myostatin expression alters fiber-type distribution and expression of myosin heavy chain isoforms in slow- and fast-type skeletal muscle. *Muscle Nerve,* 31**,** 34-40.

HEARD, D. J., NORBY, P. L., HOLLOWAY, J. & VISSING, H. 2000. Human ERRgamma, a third member of the estrogen receptor-related receptor (ERR) subfamily of orphan nuclear receptors: tissue-specific isoforms are expressed during development and in the adult. *Mol Endocrinol,* 14**,** 382-92.

HICKSON, R. C. 1980. Interference of strength development by simultaneously training for strength and endurance. *Eur J Appl Physiol Occup Physiol,* 45**,** 255-63.

JAGER, S. B., RONCHI, G., VAEGTER, C. B. & GEUNA, S. 2014. The mouse median nerve experimental model in regenerative research. *Biomed Res Int,* 2014**,** 701682.

KINSEY, S. T., HARDY, K. M. & LOCKE, B. R. 2007. The long and winding road: influences of intracellular metabolite diffusion on cellular organization and metabolism in skeletal muscle. *J Exp Biol,* 210**,** 3505-12.

LI, Y., LI, J., ZHU, J., SUN, B., BRANCA, M., TANG, Y., FOSTER, W., XIAO, X. & HUARD, J. 2007. Decorin gene transfer promotes muscle cell differentiation and muscle regeneration. *Mol Ther,* 15**,** 1616-22.

LOWRIE, M. B., KRISHNAN, S. & VRBOVA, G. 1982. Recovery of slow and fast muscles following nerve injury during early post-natal development in the rat. *J Physiol,* 331**,** 51-66.

MAURO, A. 1961. Satellite cell of skeletal muscle fibers. *J Biophys Biochem Cytol,* 9**,** 493-5.

MCPHERRON, A. C. & LEE, S. J. 1997. Double muscling in cattle due to mutations in the myostatin gene. *Proc Natl Acad Sci U S A,* 94**,** 12457-61.

NARKAR, V. A., FAN, W., DOWNES, M., YU, R. T., JONKER, J. W., ALAYNICK, W. A., BANAYO, E., KARUNASIRI, M. S., LORCA, S. & EVANS, R. M. 2011. Exercise and PGC1α-independent Synchronization of Type I Muscle Metabolism and Vasculature by ERRγ. *Cell Metab,* 13**,** 283-93.

PETTE, D. & STARON, R. S. 2001. Transitions of muscle fiber phenotypic profiles. *Histochem Cell Biol,* 115**,** 359-72.

PLYLEY, M. J., OLMSTEAD, B. J. & NOBLE, E. G. 1998. Time course of changes in capillarization in hypertrophied rat plantaris muscle. *J Appl Physiol (1985),* 84**,** 902-7.

PUTMAN, C. T., DUSTERHOFT, S. & PETTE, D. 1999. Changes in satellite cell content and myosin isoforms in low-frequency-stimulated fast muscle of hypothyroid rat. *J Appl Physiol (1985),* 86**,** 40-51.

RAMADASAN-NAIR, R., GAYATHRI, N., MISHRA, S., SUNITHA, B., MYTHRI, R. B., NALINI, A., SUBBANNAYYA, Y., HARSHA, H. C., KOLTHUR-SEETHARAM, U. & SRINIVAS BHARATH, M. M. 2014. Mitochondrial alterations and oxidative stress in an acute transient mouse model of muscle degeneration: implications for muscular dystrophy and related muscle pathologies. *J Biol Chem,* 289**,** 485-509.

RANGWALA, S. M., WANG, X., CALVO, J. A., LINDSLEY, L., ZHANG, Y., DEYNEKO, G., BEAULIEU, V., GAO, J., TURNER, G. & MARKOVITS, J. 2010. Estrogen-related receptor gamma is a key regulator of muscle mitochondrial activity and oxidative capacity. *J Biol Chem,* 285**,** 22619-29.

SCHARNER, J. & ZAMMIT, P. S. 2011. The muscle satellite cell at 50: the formative years. *Skelet Muscle,* 1**,** 28.

SCHUSTER-GOSSLER, K., CORDES, R. & GOSSLER, A. 2007. Premature myogenic differentiation and depletion of progenitor cells cause severe muscle hypotrophy in Delta1 mutants. *Proc Natl Acad Sci U S A,* 104**,** 537-42.

SHI, X. & GARRY, D. J. 2006. Muscle stem cells in development, regeneration, and disease. *Genes Dev,* 20**,** 1692-708.

TAJBAKHSH, S. & COSSU, G. 1997. Establishing myogenic identity during somitogenesis. *Curr Opin Genet Dev,* 7**,** 634-41.

VAN DER LAARSE WJ, D. T. A., LEE-DE GROOT MBE, DIEGENBACH PC 1998. Size principle of striated muscle cells. *Neth J Zool* 48: 213-223.

VASYUTINA, E., LENHARD, D. C., WENDE, H., ERDMANN, B., EPSTEIN, J. A. & BIRCHMEIER, C. 2007. RBP-J (Rbpsuh) is essential to maintain muscle progenitor cells and to generate satellite cells. *Proc Natl Acad Sci U S A,* 104**,** 4443-8.

ZAMMIT, P. S., GOLDING, J. P., NAGATA, Y., HUDON, V., PARTRIDGE, T. A. & BEAUCHAMP, J. R. 2004. Muscle satellite cells adopt divergent fates: a mechanism for self-renewal? *J Cell Biol,* 166**,** 347-57.